Communications in Physics, Vol. 30, No. 4 (2020), pp. 399-408
DOI:10.15625/0868-3166/30/4/15448

# SYNTHESIS AND ELECTROCHEMICAL CHARACTERIZATION OF $NiCo_2S_4$ NANOSHEETS/REDUCED GRAPHENE OXIDE FOR ENERGY STORAGE APPLICATIONS*

LE THI THANH TAM[1,†], DOAN THANH TUNG[1,2], NGO THANH DUNG[1,2], PHAN NGOC HONG[3], PHAM VAN HOI[4], PHAN NGOC MINH[2,3] AND LE TRONG LU[1,2,†]

[1]*Institute for Tropical Technology, Vietnam Academy of Science and Technology, 18 Hoang Quoc Viet, Cau Giay, Hanoi, Vietnam*

[2]*Graduate University of Science and Technology, Vietnam Academy of Science and Technology*

[3]*Center for High Technology Development, Vietnam Academy of Science and Technology*

[4]*Institute of Materials Science, Vietnam Academy of Science and Technology*

[†]*E-mail:* thanhtam.le95pt@gmail.com; ltlu_itims@yahoo.com

*Received 31 August 2020*
*Accepted for publication 12 September 2020*
*Published 20 November 2020*

**Abstract.** *In this present study, $NiCo_2S_4$-rGO (NCS-rGO) composites were fabricated by mixing active materials including NCS and rGO individually using polyvinylpyrrolidone (PVP) as a binder to form a homogeneous mixture. Therein, rGO was prepared by modified Hummer's method while NCS nanosheets were successfully synthesized by a thermal decomposition method using 1-dodecanethiol (DDT) as a sulfur source. The NCS-rGO composites based electrode was then produced using a 3D printing technique making it easy to design electrodes with the desired shape. The morphology and elemental composition of electrode components are characterized by energy dispersive X-ray analysis (EDX) and scanning electron microscopy (SEM). The electrochemical activity of the NCS-rGO electrode was studied in the three electrode configuration in 6M KOH electrolyte by CV, GCD and EIS measurement. The obtained results indicate that the combination of NCS nanosheets and rGO could improve the electronic conductivity of individual materials, enhance the electrochemical performance of the electrode. The as-prepared NCS-rGO electrode possesses a high $C_{sp}$ of 1535.8 $Fg^{-1}$ at 4 $Ag^{-1}$ with excellent cycling stability even after 2500 charge-discharge cycles, demonstrating that they are promising candidate for electrode material for high-performance energy storage devices in the future.*

Keywords: *electrode; energy storage device; $NiCo_2S_4$; reduced graphene oxide.*
Classification number: *77.84.Bw; 81.05.ue; 82.47.Uv; 88.05.Gh.*

*This paper is dedicated to the 40th anniversary of Institute for Tropical Technology

## I. INTRODUCTION

The serious impacts of global warming, climate change, environmental pollution and the depletion of fossil fuels have put urgent demands on the development of renewable energy sources and eco-friendly, advanced energy conversion - storage devices [1–4]. In order to resolve this problem, supercapacitors (SCs) and lithium ion batteries have been selected as the most promising candidates for research and development in recent years. Therein, SCs with unique properties such as higher energy density, faster charge/discharge rates, better cycle stability and longer life time have attracted tremendous attention and application wider in modern electrical products compared with traditional batteries and conventional capacitors [2, 3, 5–8].

According to the energy storage mechanisms, SCs are generally classified into two categories as electrical double layer capacitors (EDLCs) and pseudocapacitors [9]. In particular, the main factor, which contributes to the energy storage of SCs is electrode materials. Currently, the used electrode materials often contain carbon-based components (graphene, active carbon, carbon nanotubes), transition metal oxides/hydroxides (Co, Mn, Ru, Ni,...) or conductive polymer (polyaniline, polypyrrole,...) [10, 11]. However, in recent years, transition metal sulfides (NiS, CoS, $NiCo_2S_4$, $MnCo_2S_4$, etc.) have emerged as the best choice for electrode materials owing to their high conductivity and electrochemical activity, large capacitance and excellent cycle stability, exhibiting potential applications in high performance supercapacitor [12]. Among them, $NiCo_2S_4$ (NCS) with different nanostructures such as nanoparticles (NPs), nanosheets (NSs), nanorods,... is being considered as a promising electrode material for supercapacitor applications because of its outstanding electrochemical characteristics. The NCS exhibits stronger reactions compared to the corresponding single metal sulfides, due to the synergistic effect between cobalt and nickel with different valence states [13–16]. In addition, when compared to $NiCo_2O_4$, NCS displays a higher conductivity because of its lower band gap, especially sulfur ions tend to create more flexible structures than the oxygen ions making charge transportation easier [17–19]. Nevertheless, the drawback of NCS for practical applications is the complexity of the two step synthesis process, resulting in high cost of products [20–23]. Furthermore, the obtained NCS is often prone to agglomeration, which decreases the capacitive performance. In addition, improving the electrochemical stability and rate capability of NCS is still a challenge.

As well known, the introduction of carbon-based materials into active components of the electrode could enhance the electrochemical performances of SCs [24–26]. Especially, graphene with 2D structure possesses a large surface area (theoretical value of 2630 $m^2/g$), outstanding conductivity and mechanical properties, the introduced graphene into the electrochemical system not only improves conductivity, but also play a role as a matrix that facilitates the dispersion of NCS, preventing the NCS from aggregating, leading to improved electrochemical performance [27, 28]. For all the above mentioned reasons, in this paper, we report an effective method to fabricate NCS-graphene composites as electrode materials and analyze its electrochemical performance for energy storage applications.

## II. EXPERIMENT

### II.1. Chemicals

Cobalt (II) acetylacetonate 99 % (Sigma Aldrich), Nickel (II) chloride hexahydrate 99% (Xilong, China), oleylamine 70% (OLA), dodecanethiol 98% (DDT),octadecene (1-ODE), nitrosyl tetrafluoroborate 95% ($NOBF_4$) (Sigma Aldrich), dimethylformamide 99% (DMF) (Xilong, China).

Graphite flakes (Merck), $KMnO_4$ 99.5% (Merck), $H_2SO_4$ 98%, $H_2O_2$ 30%, HCl, deionized water, ascorbic acid 99% (Sigma Aldrich), polyvinylpyrrolidone (PVP) (Sigma Aldrich), n-hexane, ethanol.

### II.2. Fabrication of electrode based on rGO-sulfide nanomaterials

***Synthesis of NCS nanosheets:*** NCS nanosheets were prepared using a modified thermal decomposition method as reported previously [29, 30]. In a typical synthesis, 8 mmol Nikel (II) chloride hexahydrate, 16 mmol cobalt (II) acetylacetonate and OLA as a surfactant were mixed with 30 mL of 1-ODE in a three-neck, round bottom flask and evacuated at room temperature for 30 min. The solution was then heated to 140˚C, where 6 mL of 1- DDT as a sulfur source was quickly injected. The reaction mixture was then heated to 290˚C for 30 min with continuous stirring. The solution was allowed to cool to room temperature. The $NiCo_2S_4$ nanosheets were washed several times with a mixture of n-hexane, ethanol and centrifuged at 10000 rpm for 5 minutes to obtain a black product. Finally, $NOBF_4$ was used as an exchange ligand to modify the surface of $NiCo_2S_4$ nanosheets. At this time, the $NiCo_2S_4$ nanosheets have the ability to disperse in a polar and hydrophilic solvent such as water, DMF.

***Synthesis of reduced GO (rGO):*** GO was synthesized according to modified Hummer's method [31]. Firstly, 0.5 g graphite flake was dispersed into 50 mL $H_2SO_4$ (98%), 0.5 g $KMnO_4$ was then added gradually while stirring and the temperature was controlled at 50 $^o$C. The reaction mixture was diluted with 150 mL deionized water. After that, 25 mL $H_2O_2$ was added to the mixture. The resultant was centrifuged and washed several times with 10% HCl solution and then with deionized water to obtain GO suspension. Finally, GO was reduced with ascorbic acid to obtain rGO.

***Fabrication of NCS-rGO electrode***: The NCS-rGO electrode was fabricated by mixing 90 wt% active materials (including $NiCo_2S_4$ NSs and rGO with the ratio of 1:1) and 10 wt% PVP binder in DMF solvent to form a slurry. The slurry was coated on the graphite paper substrate of $2\times1$ cm$^2$ as the current collector by a modified 3D printer and kept for drying at around 100˚C [30].

### II.3. Characterization

The surface morphology and elemental distribution of the samples were analyzed using SEM-EDX. The phase structure of the material was determined by XRD.

The electrochemical properties of the supercapacitor electrodes were studied in a three-electrode configuration system using a 6M KOH solution including the as-prepared NCS-rGO electrode is used as the working electrode, the counter electrode is a platinum foil, and the reference electrode is a standard calomel electrode (SCE).

Electrochemical impedance spectroscopy (EIS) was performed in the frequency range of 100 kHz-10 mHz.

## III. RESULTS AND DISCUSSION

### III.1. Morphology and element composition of materials

The morphology and size of as-synthesized products were investigated by SEM technique. Figure 1a-c show the SEM images of rGO, $NiCo_2S_4$ NSs (NCS) and NCS-rGO material, respectively. From the obtained results, it can be seen that the thickness of the rGO sheets is very thin with a wrinkled silk-like morphology. Meanwhile, Figure 1b indicates the pristine $NiCo_2S_4$ nanosheets with the lateral size of 150-250 nm and the thickness approximately 10-20 nm. Figure 1c shows the good dispersion of $NiCo_2S_4$ nanosheets on the rGO surface with high density, suggesting a great combination between metal sulfides and rGO sheets. Furthermore, $NiCo_2S_4$ nanosheets also act as a supporting agent to prevent the re-stacking of rGO sheets and vice versa rGO sheets are like walls that protect $NiCo_2S_4$ nanosheets from agglomeration, thus facilitating ion transportation during the charged-discharged process, which is beneficial for improving the electrochemical properties.

The elemental composition of NCS-rGO composite is further investigated by energy dispersive X-ray spectroscopy (EDX) analysis, as presented in Figure 1d. From the EDX spectrum, it can be observed the elements are detected including C, O, Ni, Co, S and Cl, where C, O originate from rGO and the Cl element comes from the residual chlorine-containing precursor component. In addition, the Ni:Co atomic ratio of NCS-rGO is virtually 1:2, which is also equivalent to the initial molar ratio of $Ni^{2+}$ and $Co^{2+}$ used in the synthesis.

$NiCo_2S_4$ nanosheets synthesized by thermal decomposition method, will be surrounded by organic surfactants. Therefore, to perform the XRD analysis, $NiCo_2S_4$ material must be treated with $NOBF_4$. Figure 1e shows the XRD patterns of the $NiCo_2S_4$-$NOBF_4$. The diffraction peaks at $2\theta$ = 26.8, 31.6, 38.3, 50.4, 55.3, 65.1 and 69.3 were indexed as the crystal planes (220), (311), (400), (511), (440), (533) and (444) of $NiCo_2S_4$, respectively [14].

### III.2. Electrochemical properties

In order to investigate electrochemical behavior of as-prepared NCS-rGO electrode, CV, GCD and EIS measurements were performed using 6M KOH as electrolyte. Fig. 2a displays the CV curves of the NCS-rGO electrode at different scan rates from 5 to 100 $mVs^{-1}$ in the potential window of -0.9-0.1 V (vs. SCE). As can be seen that the CV curves present a quasi-rectangular shape with a weak redox peak, indicating that the capacitance can be attributed to the combination of electrical double-layer capacitance and pseudocapacitance mechanism, in which the redox peak originates from the faradaic reactions occuring with the $Co^{2+}/Co^{3+}$ and $Ni^{2+}/Ni^{3+}$ ions. Additionally, the symmetrical shape of CV curves in all scan rates exhibits good reversibility and stability of the NCS-rGO material as supercapacitor electrode. Based on CV curves, the specific capacitance ($C_{sp}$) of NCS-rGO is calculated according to the following equation [32]

$$C_{sp} = \frac{S}{2mv\Delta V}\left(Fg^{-1}\right) \tag{1}$$

where $v$ is the scan rate ($Vs^{-1}$), $m$ is the mass of the active material ($g$), $\Delta V$ is the potential window ($V$) and $S$ is the area under the CV curve.

The obtained results from Fig. 2b reveal that NCS-rGO electrode provides a high capacitance of 1069.3 F/g at 5 $mVs^{-1}$ scan rate. However the capacitance gradually decreases to 882.7,

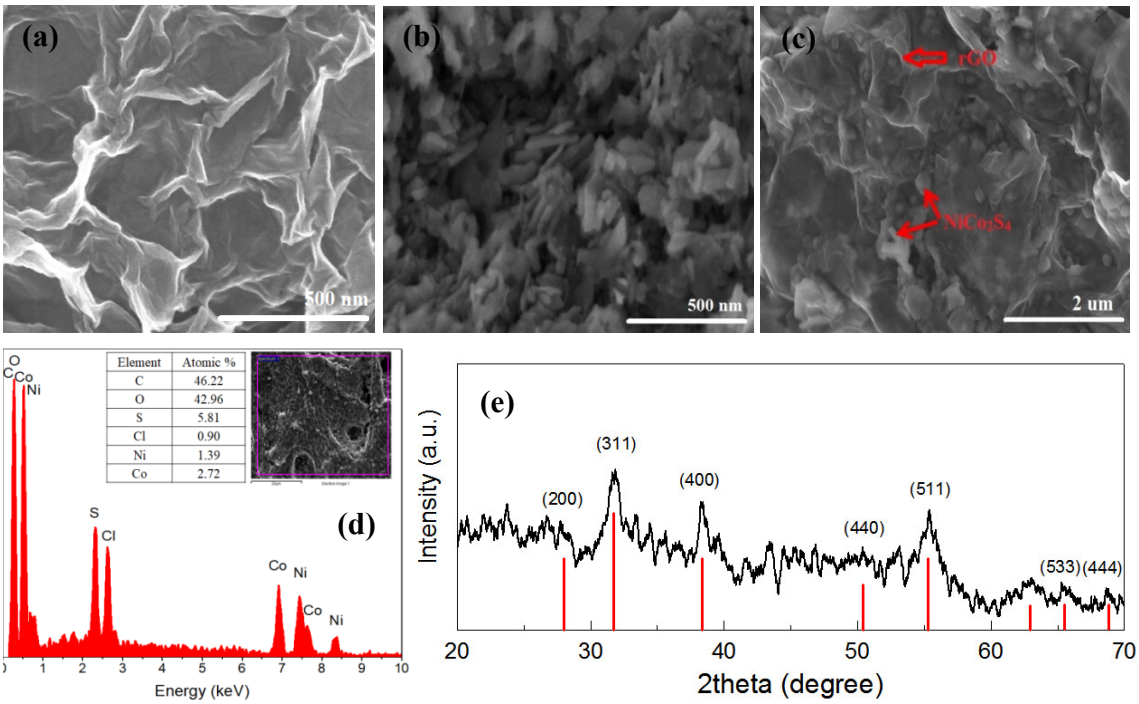


**Fig. 1.** (a-c) SEM images of rGO, $NiCo_2S_4$ NPs (NCS) and NCS-rGO material, respectively; (d) The EDX spectrum of NCS-rGO material with inset showing the percentage of elements; (e) XRD patterns of the $NiCo_2S_4$-$NOBF_4$.

713.3, 506.4, 343.9 $Fg^{-1}$ when increasing the scan rate to 10, 20, 50 and 100 $mVs^{-1}$, respectively. The capacitance drop can be explained that at the higher scan rate, the rate of electrolyte ions transfer becomes slower, limiting the diffusion of the electrolyte to access the surface electrode [33]. Simultaneously, increasing the scan rate leads to shorter redox reaction time, the redox reactions within active material occur incompletely, resulting in a decrease in capacitance [34]. Besides, the obvious increase of current density with increasing the scan rate demonstrates a good rate capability for NCS-rGO electrode.

The specific capacitance of the obtained NCS-rGO electrode was further evaluated by GCD measurements at various current densities ranging from 4 to 60 $Ag^{-1}$, as shown in Fig. 2c. As can be observed the potential drop in discharge curves, which is attributed to the contribution of the internal resistance of the electrode material. However, voltage drop is negligible at lower current density. In addition, the discharge time decreases with increased current density ranging from 4 to 60 $Ag^{-1}$. According to the GCD curves, the $C_{sp}$ can be acquired as follows [35]

$$C_{sp} = \frac{I\Delta t}{m\Delta V}\left(Fg^{-1}\right) \tag{2}$$

where $I$ represents the discharge current $(A)$ $\Delta t$ is the discharge time $(s)$ and $m$ is the mass of the active material.

Figure 2(d) shows the $C_{sp}$ values of the NCS-rGO electrode calculated from the discharge curves. As can be observed that the $C_{sp}$ as a function of current density exhibits that the specific capacitance decreases with corresponding increase in current density, which is due to slow rate of redox reactions at high current densities [36, 37]. Specifically, the NCS-rGO electrode achives the $C_{sp}$ values of 1535.8, 1251.3, 1036.1, 954.1, 891.2 and 892.5 $Fg^{-1}$ at current densities of 4, 8, 16, 25, 40 and 60 $Ag^{-1}$, respectively. Especially, the NCS-rGO electrode still retained 58% of initial $C_{sp}$ value even at a very large current density of 60 $Ag^{-1}$, indicating the excellent rate performance of electrode material.

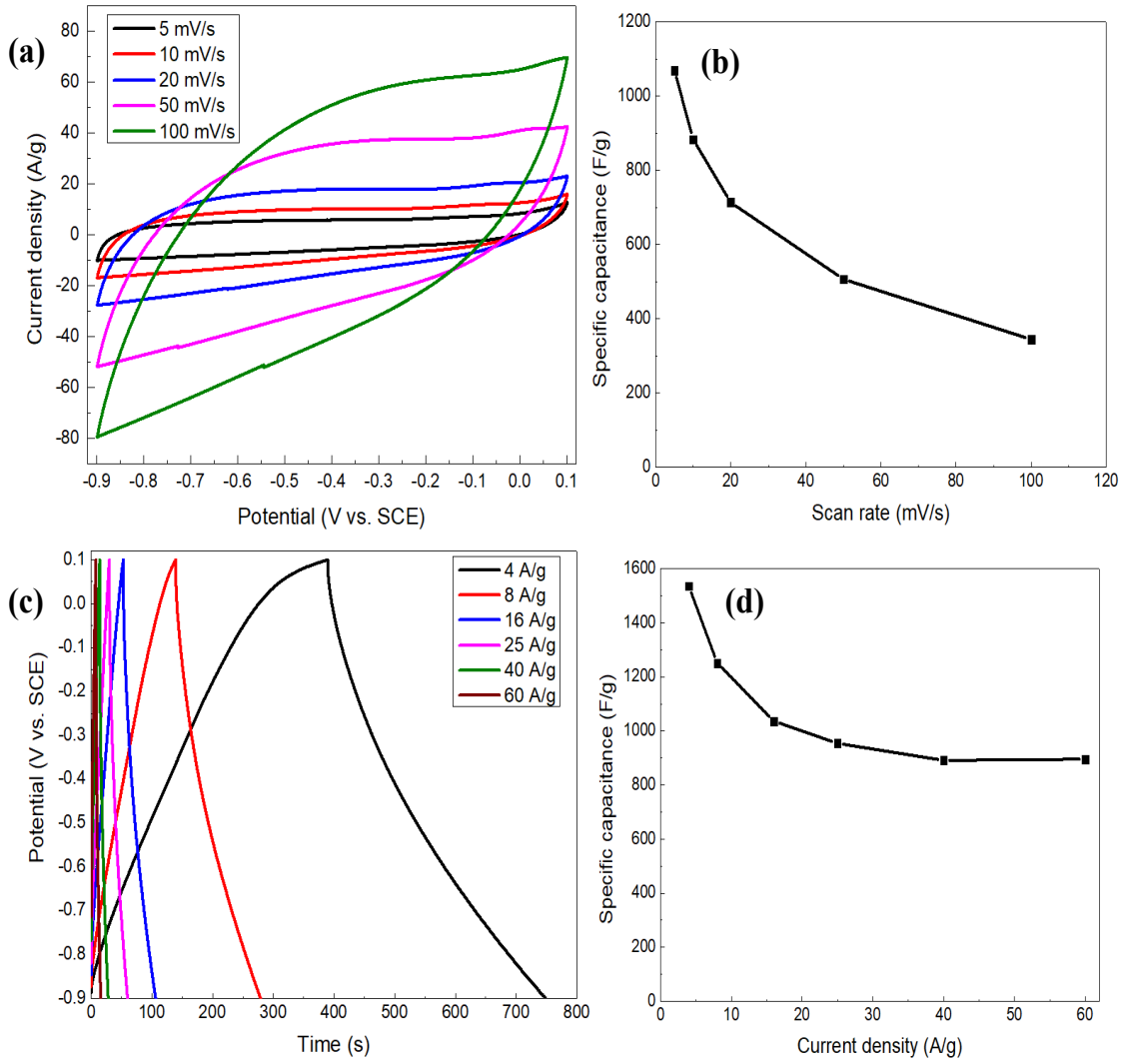


**Fig. 2.** CV curves (a) at different scan rates, (b) change in $C_{sp}$ as a function of the scan rate, GCD curves at various current densities (c), dependence of current density on $C_{sp}$ values of NCS-rGO electrode (d).

In order to further study the electrochemical characteristic of electrode material, EIS was performed to investigate charge transfer mechanism at an electrode/electrolyte interface. Fig. 3a shows the Nyquist plots of rGO, NCS and NCS-rGO electrodes, which were recorded in the frequency range of 10 mHz to 100 kHz, and the equivalent circuit according to the EIS spectra is shown in the inset Fig. 3a, where $R_s$ represents the solution resistance; CPE is the constant phase element accounting for a double-layer capacitance; $R_{ct}$ is the charge transfer resistance related to the Faradic reactions; W is the Warburg impedance coming from the ion diffusion and transport in the electrolyte [14, 38]. As observed from these plots, all the samples consist of two parts, a semicircle at high frequency and a linear line at low frequency regions. The equivalent series resistance ($R_s$) values for NCS, rGO and NCS-rGO electrode are 1.24, 1.15 and 1.09 Ω, respectively, indicating the better electronic conductivity ofNCS-rGO electrode when compared with NCS and rGO individually. Furthermore, at the high frequency range, the semicircle of NCS-rGO electrode with the smallest diameter can be found, which means that the NCS-rGO electrode represents the lowest charge transfer resistance ($R_{ct}$). Based on EIS data, $R_{ct}$ value for NCS-rGO, rGO and NCS electrodes is 0.34, 0.70 and 0.77 Ω, respectively. The small $R_{ct}$ of the NCS-rGO electrode illustrates fast ion diffusion and easy electron transport. Besides, in the Nyquist plots, the slope of NCS-rGO electrode at the low frequency region called as Warburg impedance (W) is greater than the NCS and rGO electrodes, revealing the better electrolyte ion diffusion within NCS-rGO electrode during the redox reactions, which is a suggestion of an ideal capacitive behavior of NCS-rGO materials.

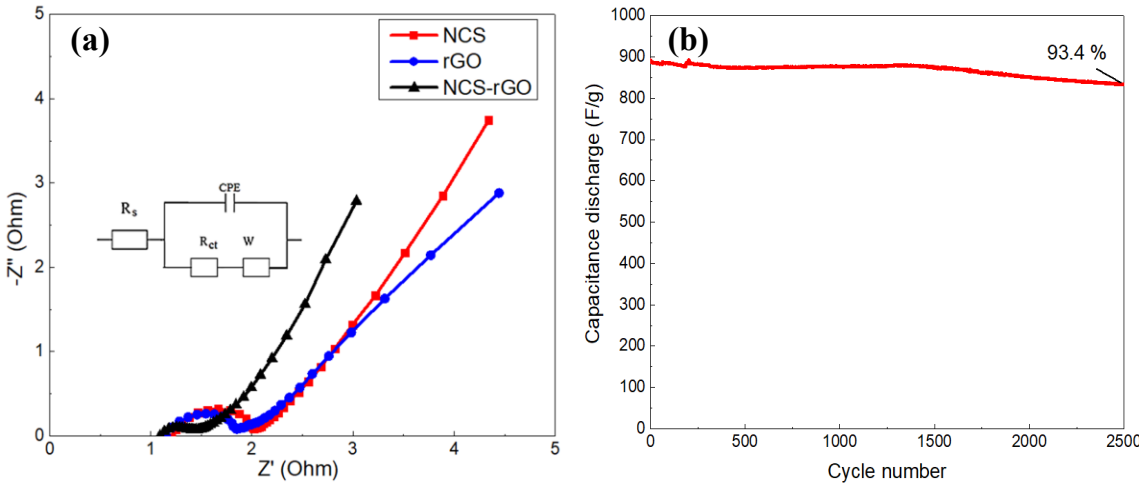


**Fig. 3.** EIS measurement (Nyquist plot) of rGO, NCS, NCS-rGO samples (a) and cycling performances of the NCS-rGO electrode at a constant current density of 60 A $g^{-1}$ for 2500 cycles (b).

Electrochemical stability of the electrode is an important factor for energy storage application of SCs. For this reason, in this work, the cycling stability of the NCS-rGO electrode was measured at the constant current density of 60 $Ag^{-1}$, and the result is presented in Fig. 3b. The specific capacitance retains 93.4% of its initial value after 2500 charge-discharge cycles, indicating

excellent cyclic stability of the material. In summary, NCS-rGO electrode displays high specific capacitance, large rate capability and great cycle stability. This good performance was ascribed to the synergistic effect between rGO and NCS nanosheets.

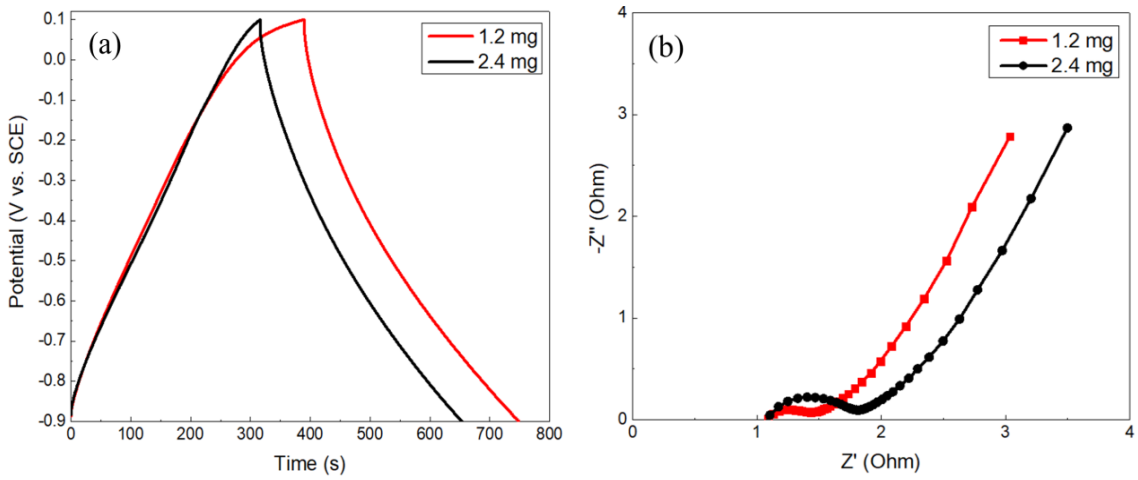


**Fig. 4.** GCD curves (a) and EIS spectra (b) of NCS-rGO electrodes with different mass loadings at a current density of 4 $Ag^{-1}$.

To further study on the electronic conductivity and electrochemical activity of the NCS-rGO material, the specific capacitance of the NCS-rGO electrode with different material loadings are evaluated. Fig. 4 shows GCD curves and EIS spectra of the NCS-rGO electrode with different material loadings at the current density of 4 $Ag^{-1}$. As can be observed from Fig. 4b, $R_s$ value is nearly unchanged while $R_{ct}$ increases with increasing material loadings. This is consistent with the decrease in $C_{sp}$ value obtained from the discharge curve presented in Fig. 4a. However, the decline of the $C_{sp}$ value is negligible, demonstrating the good conductivity and high electrochemical activity of the NCS-rGO material, indicating that NCS-rGO material is suitable for the electrode material of supercapacitor.

## IV. CONCLUSIONS

In summary, $NiCo_2S_4$-rGO nanocomposites were successfully fabricated through a simple, easy to scale-up approach in laboratory conditions. The obtained $NiCo_2S_4$ is spherical with the size of hundreds of nanometers while we obtained a sheet-like $NiCo_2S_4$ structure, which is benificial for transportation and anchoring of charged ions during the charged-discharged process. The as-prepared $NiCo_2S_4$-rGO material revealed the outstanding electrochemical behaviors such as good rate capability, a high specific capacitance of 1535.8 $Fg^{-1}$ at the current density of 4 $Ag^{-1}$, excellent cycling stability with 93.4 % of initial capacitance retention at the high current density of 60 $Ag^{-1}$ after 2500 charge-discharge cycles. The results are approximately equal to, even superior to the results of reported papers previously [39–43]. It obviously indicates the great potential of $NiCo_2S_4$-rGO composite as electrode materials for the next generation electrochemical energy storage devices.

## ACKNOWLEDGEMENT

This work was supported by the Vietnam National Foundation for Science and Technology Development (NAFOSTED) under Grant Number 103.02- 2018.66.

## REFERENCES

[1] A. S. Arico, P. Bruce, B. Scrosati, J.M. Tarascon, W.V. Schalkwijk, *Nat. Mater.* **4** (2005) 366.
[2] C. Liu, F. Li, L. P. Ma, H. M. Cheng, *Adv. Mater.* **22** (2010) E28–E62.
[3] N. Garg, M. Basu, A. K. Ganguli, *J. Phys. Chem. C* **118** (2014) 17332.
[4] S. Zhang, N. Pan, *Adv. Energy Mater.* **5** (2015), 1401401.
[5] P. Simon, Y. Gogotsi, *Nat. Mater.* **7** (2008) 845.
[6] K. Xu, R. Zou, W. Li, Q. Liu, X. Liu, L. An, J. Hu, *J. Mater. Chem. A* **2** (2014) 10090.
[7] L. L. Zhang, X. Zhao, *Chem. Soc. Rev.* **38** (2009) 2520.
[8] J. R. Miller, P. Simon, *Sci. Mag.* **321** (2008) 651.
[9] A. Wang, H. Wang, S. Zhang, C. Mao, J. Song, H. Niu, Y. Tian, *Appl. Surf. Sci.* **282** (2013) 704.
[10] Z. Fan, J. Yan, T. Wei, L. Zhi, G. Ning, T. Li, F. Wei, *Adv. Funct. Mater.* **21** (2011) 2366.
[11] W. Peng, H. Li, S. Song, *ACS Appl. Mater. Interfaces*, **9** (2017) 5204.
[12] P. Kulkarni, S. K. Nataraj, R. G. Balakrishna, D. H. Nagaraju, M. V. Reddy, *J. Mater. Chem. A.* **5** (2017) 22040–22094.
[13] S. J. Peng, L. L. Li, C. C. Li, H. T. Tan, R. Cai, Yu H, S. Mhaisalkar, M. Srinivasan, S. Ramakrishna, Q. Y. Yan, *Chem. Commun.* **49** (2013) 10178.
[14] X. Cai, X. Shen, L. Ma, Z. Ji, L. Kong, *RSC Advances* **5** (2015) 58777.
[15] J. Li, S. Xiong, Y. Liu, Z. Ju, Y. Qian, *ACS Appl. Mater. Interfaces* **5** (2013) 981.
[16] T. Chen, Y. Tang, W. Guo, Y. Qiao, S. Yu, S. Mu, F. Gao, *Electrochimica Acta* **212** (2016) 294.
[17] H. Nan, J. Han, Q. Luo, X. Yin, Y. Zhou, Z. Yao, X. Zhao, X. Li, H. Lin, *Appl. Surf. Sci.* **437** (2018) 227.
[18] H. Chen, J. Jiang, L. Zhang, H. Wan, T. Qi, D. Xia, *Nanoscale* **5** (2013) 8879.
[19] Surjit Sahoo, Chandra Sekhar Rout, *Electrochemica Acta*, **220** (2016) 57.
[20] J. Pu, F. L. Cui, S. B. Chu, T. T. Wang, E. H. Sheng, Z. H. Wang, *ACS Sustainable Chem. Eng.* **2** (2014) 809.
[21] Y. F. Zhang, M. Z. Ma, J. Yang, C. C. Sun, H. Q. Su, W. Huang, X. C. D, *Nanoscale*, **6** (2016) 9824.
[22] L. Yu, L. Zhang, H. B. Wu, X. W. D. Lou, *Angew. Chem. Int. Ed. Engl*, **53** (2014) 3711.
[23] J. W. Xiao, X. W. Zeng, W. Chen, F. Xiao, S. Wang, *Chem. Commun.* **50** (2014) 9596.
[24] Q. Li, N. Mahmood, J.H. Zhu, Y.L. Hou, S.H. Sun, *Nano Today* **9** (2014) 668.
[25] M. J. Zhi, C. C. Xiang, J. T. Li, M. Li and N. Q. Wu, *Nanoscale* **5** (2013) 72.
[26] W. M. Du, Z. Y. Wang, Z. Q. Zhu, S. Hu, X. Y. Zhu, Y. F. Shi, H. Pang, X. F. Qian, *J. Mater. Chem. A* **2** (2014) 9613.
[27] X. Huang, Z. Y. Yin, S. Wu, X. Y. Qi, Q. He, Q. Zhang, Q. Yan, F. Boey, H. Zhang, *Small* **7** (2011) 1876.
[28] C. C. Xiang, M. Li, M. J. Zhi, A. Manivannan, N. Q. Wu, *J. Power Sources*, **226** (2013) 65.
[29] Le T. T. Tam, Nguyen V. Hung, Doan T. Tung, Ngo T. Dung, Hoang T. Dung, Pham T. Nam, Phan N. Minh, Phan N. Hong, Le T. Lu, *Vietnam J. Sci. Technol.* **57** (2019) 58.
[30] Doan T. Tung, Le T. T. Tam, Hoang T. Dung, Ngo T. Dung, Nguyen T. Dung, Thai Hoang, Tran D. Lam, Phan N. Minh, Tran V. Thu, Phan N. Hong, Le T. Lu, *J. Electron. Mater.* **49** (2020) 4671.
[31] K. Fu, Y. Wang, C. Yan, Y. Yao, Y. Chen, J. Dai, S. Lacey, Y. Wang, J. Wan, T. Li, Z. Wang, Y. Xu, L. Hu, *Adv. Mater.* **28** (2016) 2587.
[32] S. Sahoo, C. S. Rout, *Electrochimica Acta* **220** (2016) 57.
[33] W. M. Du, Z. Q. Zhu, Y. B. Wang, J. N. Liu, W. J. Yang, X. F. Qian, H. Pang, *RSC Adv.* **4** (2014) 6998.
[34] M. B. Zakaria, M. Hu, R. R. Salunkhe, M. Pramanik, K. Takai, V. Malgras, S. Choi, S. X. Dou, J. H. Kim, M. Imura, S. Ishihara, Y. Yamauchi, *Chem. A Eur. J.* **21** (2015) 3605.
[35] C. Mondal, M. Ganguly, P. K. Manna, S. M. Yusuf and T. Pal, *Langmuir*, **29** (2013), 9179.
[36] S. Sahoo, C. S. Rout, *Electrochimica Acta*, **220** (2016) 57–66.
[37] T. Morishita, Y. Soneda, H. Hatori, M. Inagaki, *Electrochim. Acta*, **52** (2007) 2478.
[38] Y. H. Li, L. J. Cao, L. Qiao, M. Zhou, Y. Yang, P. Xiao, Y. H. Zhang, *J. Mater. Chem. A* **2** (2014) 6540.

[39] Z. Li, X. Ji, J. Han, Y. Hu, R. Guo, *J. Colloid Interface Sci.* **477** (2016) 46.
[40] X. Yang, H. Niu, H. Jiang, Z. Sun, Q. Wang, F. Qu, *ChemElectroChem*, **5** (2018) 1576.
[41] Y. Wu, M. Yan, L. Sun, W. Shi, *New J. Chem.* **42** (2018), 16174.
[42] W. Peng, H. Chen, W. Wang, Y. F. Huang, G. Han, *Curr. Appl. Phys.* **20** (2020) 304.
[43] N. V. Hoa, P. A. Dat, N. V. Hieu, T. N. Le, N. C. Minh, Ng. V. Tang, D. T. Nga, T. Q. Ngoc, *Diam. Relat. Mater.* **106** (2020), 107850.